

Dependence of APE simulations on vertical resolution
with the Community Atmospheric Model, Version 3

David L. Williamson

National Center for Atmospheric Research*, Boulder, Colorado

Submitted to *Journal of the Meteorological Society of Japan*
special issue on the Aqua-Planet Experiment

22 July 2009

Revised 5 October 2009

*The National Center for Atmospheric Research is sponsored by the National Science Foundation.

Corresponding author's address:

David L. Williamson

National Center for Atmospheric Research

Box 3000

Boulder, CO 80307-3000

e-mail: wmson@ucar.edu

Abstract

The convergence of the zonal averaged equatorial precipitation with increasing vertical resolution in simulations with Community Atmosphere Model (CAM3) Eulerian spectral transform and finite volume dynamical cores is considered. The cores are both coupled to the standard CAM3 parameterization package. With the standard CAM3 26 level grid, the two versions converge to different states when the horizontal resolution alone is refined; the spectral transform to a single precipitation maximum and the finite volume to a double. With increasing vertical resolution both converge to a double structure. However, in the subsidence regions the high vertical resolution simulations have a very different climate balance and parameterized forcing than the lower resolution simulations and thus they do not represent the expected climate associated with the lower resolution dynamical cores.

The cause of the different parameterized forcing is studied by considering the evolution of the 60-level model starting from a state created by the 26-level model. The cause is shown to be the discrete approximations in the shallow convection. When the 60-level model is presented with an initial state interpolated from a 26-level model state, the columns are stable by the discrete test in the shallow convection, even though they are unstable when the discrete calculation is based on the coarser 26-level grid. The Planetary Boundary Layer parameterization pumps water vapor into the lower troposphere, low clouds increase to unrealistic levels and force strong longwave radiative cooling. This destabilizes the column until the discrete test is satisfied on the 60-level grid and the shallow convection becomes active again. However the simulated state is by then very different and unlike the earth's atmosphere. Similar unrealistic behavior has been seen in earth-like simulations.

1 Introduction

Recently Williamson (2008a) showed that when horizontal resolution alone was increased in Aqua Planet Experiment (APE) simulations with the Community Atmosphere Model version 3 (CAM3), the equatorial precipitation appeared to be converging with both the model version based on the Eulerian spectral transform dynamical core and the version based on the finite volume core, the sub-grid scale parameterizations being the same. However, the simulations from the two model versions appeared to be converging to different states in the equatorial region. The Eulerian spectral dynamical core simulation was converging to a single precipitation maximum centered on the equator and the finite volume to double precipitation maxima spanning the equator. Although the simulations had not actually converged by the highest resolutions run, T340 for the spectral transform and 0.5° for the finite volume, there was no indication that they were converging toward the same solution. Here, convergence is defined as the two highest resolutions of a single configuration producing the same solution for the features being considered.

Figure 1 shows the zonal average precipitation from these simulations for the equatorial region. The dots on the lines indicate the grid point locations. The sub-grid scale parameteri-

zations and associated free parameters were the same in all simulations as were the parameterization time steps. The double structure of the simulation with the finite volume core becomes well resolved with increasing resolution. This was not the case in earlier simulations with the semi-Lagrangian version of the Community Climate Model version 3 (CCM3), the predecessor of CAM3. In that model a double structure became narrower with increasing horizontal resolution and always remained a grid interval structure (Williamson and Olson, 2003).

In the following we consider the convergence of the two model versions with increasing vertical resolution. The two will be seen to converge to the same state (Section 3), namely the double precipitation maxima spanning the equator. This state however has some dubious properties in the subsidence regions which have also been seen in Earth-like simulations with the CAM at higher vertical resolution. The most obvious being very large cloud amounts at the top of the Planetary Boundary Layer (PBL) leading to excessive radiational cooling. The aqua-planet formalism is ideal to investigate the cause of this common problem because it occurs over a relatively large, homogeneous region in that configuration. Averaging over the larger, homogeneous area reduces the noise and allows shorter experiments and clearer signals. Medeiros and Stevens (2010) also conclude that aqua-planets are advantageous to examine certain atmospheric phenomena in models, including comparisons with atmospheric observations. Section 4 considers the processes involved in the evolution of the 60-level model from a state created by the 26-level model. This evolution exposes the cause of the high resolution problem. It is due to the discrete approximations in the shallow convection parameterization. Finally it is argued in Section 5 that the 60-level state cannot be used as a surrogate for what the 26-level state should be because the parameterized forcing is very different between the 60-level and 26-level simulations. Thus we cannot conclude that the 26-level finite volume core is better than the 26-level spectral transform core.

2 Model and Experiment Descriptions

The simulations described above and in the following were performed with the CAM3 using two different dynamical cores. In one case the horizontal dynamical approximations are based on the traditional Eulerian spectral transform method (Machenhauer, 1979) and in the other on finite volume approximations (Lin and Rood, 1996, 1997). The spectral transform based core employs a hybrid sigma-pressure vertical coordinate developed by Simmons and Strüfing (1981) and vertical energy conserving finite difference approximations detailed in Collins et al. (2004).

The finite volume core uses a Lagrangian vertical coordinate (Lin, 2004) that moves up and down with the flow. The state variables are remapped conservatively to the spectral transform core’s hybrid vertical coordinate before the parameterization calculations. Therefore, in the two model versions the parameterizations are calculated on the same vertical grid. In addition, the parameterization calculation uses the same time step, 5 minutes, in all simulations discussed here since the parameterization suite is very sensitive to the time step (Williamson, 2008a).

All experiments described here use the standard CAM3 parameterization suite. The planetary boundary layer (PBL) is parameterized following Holtslag and Boville (1993). Moist convection is parameterized by the Zhang and McFarlane (1995) deep scheme followed by the Hack (1994) scheme for shallow convection. The treatments of microphysics and cloud condensation are discussed in Boville et al. (2006). The prognostic cloud water scheme is presented in Rasch and Kristjánsson (1998) and Zhang et al. (2003). Details of the other processes are supplied by Collins et al. (2006) and references therein. A complete technical description of CAM3 and the two dynamical cores considered here is provided by Collins et al. (2004).

The experiments presented here are all based on the “CONTROL” case of Neale and Hoskins (2000) and of the Aqua Planet Experiment (APE) (<http://www.met.reading.ac.uk/~mike/APE/>). The specified zonally symmetric SST in °C is given by $27 \left[1 - \sin^2(3\varphi/2) \right]$ for latitude φ between $\pm\pi/3$ and 0 for $|\varphi| \geq \pi/3$.

To produce the mean climate of the model, simulations start from a state taken from a previous aqua-planet simulation, possibly interpolated from a different resolution, and are run for 14 months. When starting from a closely related aqua-planet state, the model transitions to its own aqua-planet climate in less than 2 months. The climate is given by the average over the last 12 months which is adequate for the statistics considered here.

3 Climate as function of vertical resolution

In the horizontal convergence study of Williamson (2008a) described above in the introduction the vertical resolution was held fixed at the CAM3 standard 26 levels. The obvious question is: do simulations from the two variants of CAM3 converge to the same state when the vertical resolution is also increased? The vertical approximations in the two dynamical cores are very different.

In a normal convergence study in computational fluid dynamics all dimensions are refined simultaneously. However that approach is beyond our available resources. Therefore we refine the

vertical resolution alone at a fixed modest horizontal resolution which, although not the highest in the horizontal resolution study, is adequate to clearly define the equatorial structures (Fig. 1). These are T85 for the spectral transform version and 1° for the finite volume. Williamson (2008b) showed that APE simulations at these resolutions were equivalent for many climatological statistics including ones involving tropical variability. An exception was the morphology of the mean Hadley circulation in the equatorial region.

We consider the convergence of simulations at these horizontal resolutions as the vertical resolution increases from 26 to 30 and 60 vertical levels. The 26 levels are the standard used in CAM3. The 26 levels were an augmentation of the 18-level vertical grid used for CCM3 (Kiehl et al., 1996), the predecessor of CAM3. The levels added to the 18-level grid basically halved the grid intervals between 200 and 50 mb but made little change below 500 mb. Williamson et al. (1998) showed that the 26 levels gave convergent Held-Suarez (Held and Suarez, 1994) simulations of the tropical tropopause temperature and reduced the tropical tropopause temperature bias compared to the 18-level model climate in earth-like simulations with CCM3. Levels were not added below 500 mb at that time because there were indications that the parameterizations were sensitive to the resolution near the surface. In preparation for CAM3 the 30-level grid was designed in which the number of levels below 700 mb in the 26-level grid was increased from 5 to 9. It was thought that the increased resolution should be beneficial to the PBL parameterization but it proved to be problematical when developing CAM3 and was withdrawn from consideration. The problem will be seen in the following. The 60-level grid essentially halves the 30 level grid intervals, although not uniformly since it is desirable that the vertical grid intervals vary smoothly with height (Williamson et al., 1998). The 60-level grid has been used recently by Hannay et al. (2009). The nominal pressure levels of the hybrid vertical coordinates ($A_{p_0}+B_{p_s}$, $p_0=p_s=1000$ mb) of these three grids are shown below 500 mb in Figure 2.

Figure 3 shows the simulated equatorial precipitation from simulations with the 26-, 30- and 60-level grids. Both versions of CAM3 appear to be converging to a double structure. The structure from the spectral transform simulation appears to be wider than that from the finite volume but the underlying spectral transform Gaussian grid on which the data are plotted is 1.4° compared to 1.0° for the finite volume version, and the spectral transform points are shifted half a grid interval away from the equator. It would seem natural to assume that this double structure would be more correct for the lower resolution and that therefore the finite volume dynamical core was more accurate than the spectral at lower resolution. However we will argue in the following that this is not necessarily the case because the parameterized forcing of the

dynamical cores becomes very different at the higher vertical resolutions.

We now consider the simulations in the subsidence region poleward of the upward branch of the Hadley circulation and precipitation maxima, i.e. the source region for much of the water vapor which is transported into the equatorial region to drive the Hadley circulation. We consider the T85 spectral transform simulations. In this region the behaviors examined in the following are very similar in simulations with the 1° finite volume core. Figures 4a, b and c show the relative humidity, cloud fraction and longwave radiative heating, respectively, averaged over latitudes $7.5^\circ \leq |\varphi| \leq 17.5^\circ$ for the 26-, 30- and 60-level simulations. At 900 mb the relative humidity increases from 88% to 93% to 96% going from 26 to 30 to 60 levels. The cloud fraction increases from 0.2 to 0.45 to 0.7, and above the cloud layer the magnitude of the longwave cooling increases from -3 K/day to -10 K/day to -14 K/day. The large cloud fraction and strong radiative cooling at higher resolutions are unrealistic compared to the earth's atmosphere, but these are simulations of an aqua-planet which cannot be observed. However the same problematic behavior is seen with 30-levels in earth-like simulations and it has not been possible to tune around this problem with the CAM3 parameterizations (J. Hack, personal communication; R. Neale and C. Hannay, personal communication). A component of the cloud parameterization depends on a specified minimum relative humidity (Collins et al., 2004). In that component, the diagnostic cloud fraction increases from 0.0 to 1.0 as the relative humidity increases from the specified minimum value to 100%. We will see why the parameterizations could not be tuned to give satisfactory simulations in the next section. First, however, we examine the climatology of the dominant specific humidity parameterization terms in this region.

Figures 4d and e show the climatological parameterized PBL and moist processes specific humidity tendencies, respectively. The collection identified as moist processes includes the deep and shallow convection parameterizations and the prognostic cloud water parameterization. Consider the 26-level simulation first. The PBL parameterization deposits water vapor around 930 mb and the moist processes remove about two-thirds of that and move some up to the next model level at 865 mb. This behavior has been described in earth-like simulations with CAM3 by Hannay et al. (2009).

The 30-level and 60-level simulations behave similarly, although both processes are stronger and of finer scale with the level of maximum PBL deposition and moist process depletion occurring higher at a grid level which lies between levels of the next lower resolution grid. (The grid points are indicated by dots on the plotted lines.) This behavior is not unlike that often seen with increased resolution in sub-resolved calculations. In general, these parameterization

moisture tendencies look consistent with increasing resolution however the model state driving them seen in Figs. 4a, b and c becomes unreasonable at the higher resolutions. We note that the parameterization temperature tendencies are very different at higher resolutions as indicated by the radiative heating (Fig. 4c.)

4 Transition of 60-level simulation from a 26-level initial state

How do the higher resolution simulations attain very different states while the moisture forcing by the PBL and moist process parameterizations look rather similar? We answer this question in this section by examining the temporal evolution of the 60-level model initialized with a state from the 26-level simulation. The evolution of the 30-level model initialized with a state from the 26-level simulation is very similar to the 60-level model evolution. We will see that the 60-level model applied to the 26-level state initially behaves very differently from its 60-level climate.

Figures 5a, b and c show the evolution of temperature, specific humidity and relative humidity, respectively, over the first two days of the transition of the 60-level model from the initial 26-level state. Temperature and specific humidity are shown as changes from the initial state. Below 850 mb the model cools and moistens, and both trends contribute to increased relative humidity.

Figures 5d, e and f show the accompanying change in the three types of clouds in the model which contribute to the total cloud fraction. The graphed lines represent one hour averages, ending at the hour indicated. The dashed line labeled “0 hr” is the 1 hr value from a matching 26-level run. The 26-level values vary little with time and the initial value indicates the basic 26-level behavior. Collins et al. (2004) detail the diagnostic cloud parameterization. It consists of three components referred to as convective clouds, relative humidity clouds and stratus clouds. The convective cloud fraction (C_{CONV}) is related to the updraft mass flux in the deep and shallow convection parameterizations. The 26-level convective cloud fraction is around 0.16 at 870 mb whereas initially the 60-level value is about 0.04. In the 60-level integration it increases over the two days to reach a value of 0.24 at 890 mb. The so called relative humidity clouds (C_{RH}) are also small initially, around 0.04, and increase to 0.40 at 890 and 905 mb at two days in contrast to the 26-level values which are around 0.04. The relative humidity clouds are small to start with because the relative humidity is below 90% at many points. The initial zonal average in

Fig. 5c is 87%. It then increases to 95% over the two days. The relative humidity clouds are diagnosed based on relative humidity by

$$C_{\text{RH}} = \left(\frac{RH - RH_{\text{min}}}{1 - RH_{\text{min}}} \right)^2 \quad (1)$$

where the relative humidity RH is expressed as a fraction and RH_{min} is 0.91 for low clouds below 750 mb. The stratus clouds (C_{ST}) increase from close to 0.0 to 0.10 in the 60-level run while the 26-level value is small at 0.02. The stratus clouds are diagnosed using an empirical relationship based on the stratification between the surface and 700 mb from Klein and Hartmann (1993). These stratus clouds are not an important component of the total in this region.

The three types of cloud combine to give a total cloud fraction by

$$C_{\text{TOT}} = \min(\max(C_{\text{RH}}, C_{\text{ST}}) + C_{\text{CONV}}, 1). \quad (2)$$

(The formula for C_{TOT} on page 102 of Collins et al. (2004) is incorrect.) In the subsidence region being examined the total cloud is essentially the sum of the convective and relative humidity clouds. The total cloud fraction is shown in Fig. 5g. In the 60-level integration it increases from around 0.06 to 0.64 at 890 and 905 mb in two days whereas the 26-level value is at most 0.20. The cloud liquid water (Fig. 5h) also increases in the 60-level integration from 0.03 g/kg to 0.18 g/kg compared to 0.03 g/kg in the 26-level integration. Thus the diagnosed cloud fraction does not consist of “empty clouds” with no cloud water and the clouds have a significant radiative effect as seen in Fig. 5i. After two days the radiative cooling above the clouds at 856 and 873 mb is greater than 8 K/day compared to a rather vertically uniform 2 K/day in the 26-level integration.

In the 60-level integration why does the relative humidity increase to such large values which in turn lead to the unreasonably large cloud fraction and strong radiative cooling? Figures 6a, b and c show the two-day evolution of the parameterized specific humidity tendencies. Once again, the dashed line labeled “0 hr” represents the 26-level simulation value. In the 60-level integration the PBL (Fig. 6a) shows little variation over the two days. The maximum moves upward from 930 mb to 905 mb, a level between the 26-level ones, but it shows minimal variation in strength. The shallow convection (Fig. 6b), ultimately the dominant component of the moist processes, is zero initially in the 60-level integration whereas in the 26-level integration it is -4.0 g/kg/day at 930 mb. As seen in the terms in the climate averages (Figs. 4d and e) in the 26-level integration the PBL deposits water vapor in lower troposphere around 930 mb and the shallow convection removes it, moving some of it up to the next layer. In the 60-level transient integration (Figs.

6a and b) the PBL also deposits water vapor in lower troposphere but the shallow convection is initially inactive, and does not remove any. Thus the specific humidity increases as seen in Fig. 5b. Gradually, over the two days, the shallow convection does become active again resembling the 26-level value at the end of the period. Since initially the shallow convection does not remove the water vapor deposited by the PBL, the prognostic cloud water parameterization (Fig. 6c) attempts to do so initially, but rather weakly at 2.0 g/kg/day. In the 26-level model this term is rather small but provides a small source higher up. In the 60-level integration this term appears to move the water vapor down. It does this through a combination of processes. The removal at 930 mb is a conversion of vapor to cloud liquid water. This liquid is then transported downward by the resolved scale transport (subsidence). At the lower levels some of the cloud liquid water is evaporated back to vapor. Overall however this process is relatively unimportant. Similarly the deep convection (not shown) does not contribute in this region. Essentially, the specific humidity increases initially due to the PBL deposition. This leads to increased clouds which in turn lead to increased radiative cooling making the atmosphere more unstable. This drives shallow convection which also transports additional moisture upward resulting in a vicious cycle.

The remaining question is why does the shallow convection turn off in the 60-level model when provided with the 26-level state? The shallow convection is active if the moist static energy at a level exceeds the saturated moist static energy at the level above (Hack, 1994). The moist static energy, h , is

$$h = C_p T + gz + Lq \quad (3)$$

where T is temperature, z is geopotential height, q is specific humidity, g is the acceleration due to gravity, C_p is the specific heat capacity of dry air and L is the latent heat of vaporization. The saturated moist static energy, h^* , is

$$h^* = C_p T + gz + Lq^* \quad (4)$$

where q^* is the saturated specific humidity. The shallow convection is active when

$$h_{k+1} + pert > h_k^* \quad (5)$$

where k is the vertical grid index increasing downward and $pert$ denotes a perturbation that is added when the convection is rooted in the boundary layer. Figures 6d and e show the fraction of points in this region that are unstable as a function of time and level for the 26-level and 60-level transition experiments, respectively. The 26-level fraction is around 0.45 at 930 mb and

is reasonably constant over the two days. The 60-level fraction, on the other hand, is basically 0 initially, increasing gradually over the first few hours, and eventually becoming almost 0.8 after two days. The 26-level state is not unstable when sampled with the 60 discrete levels. Figure 7 illustrates how this comes about for a single point at 7.7° latitude and 243.3° longitude. Ignoring the perturbation, this is the most unstable point in the 26-level model with the 26-level initial data. The moist static energy, h , is plotted as the solid line and the saturated moist static energy, h^* , as the dashed line. The vertical lines originating along the moist static energy curve elevate it to the next model level above. Thus, ignoring the perturbation term, if the top of the vertical segment is to the right of the dashed line, the point is unstable and convection is triggered. If it is to the left convection does not occur. In the 26-level model, the third model level from the bottom is unstable at 0 hr (Fig. 7a). But when calculated for the 60-level model on the data interpolated from the 26-level data, the column is stable everywhere (Fig. 7b), and shallow convection does not occur. At one and two hours the column continues to be stable (Fig. 7c and d). At three hours the seventh point from the bottom is slightly unstable (Fig. 7e). By 6 hours several points in the column are unstable (Fig. 7f) and the shallow convection has resumed.

We now summarize the evolution of the 60-level simulation starting from 26-level data created by a 26-level simulation. The shallow convection initially turns off because at the increased vertical resolution the columns are stable by the discrete test upon which the parameterization is based. The PBL parameterization deposits water vapor between 850 and 900 mb. Neither the deep convection nor the prognostic cloud water parameterizations act to replace the inactive shallow convection in removing some of the water vapor. Thus the relative humidity increases between 850 and 900 mb and the relative humidity clouds start to form and increase in response to the moisture increase. The clouds lead to increased longwave radiation cooling which destabilizes the atmosphere enough so that the shallow convection then turns back on. The convection transports additional moisture upward from the PBL deposition layer which leads to even more convective and relative humidity clouds and stronger radiative cooling in a vicious cycle. Ultimately the 60-level equilibrium is established in which the PBL and shallow convection moisture tendencies do not appear to be very different from the 26-level behavior. However, by then the atmospheric state in the 60-level simulation is unlike the earth's atmosphere. Similar unreasonable states form in earth-like simulations with CAM3 at higher vertical resolution. The shallow convection parameterization requires these unreasonable states in order to become active with 60 levels and thus appears to be inaccurate at higher vertical resolution. This is the opposite

of the behavior we normally expect of approximations applied at higher resolution. Since the dynamical approximations and many of the other parameterizations become more accurate at higher resolutions, the shallow convection parameterization should be improved or replaced to allow increased vertical resolution. It is being replaced in the next version of the CAM.

5 Implication for convergence with vertical resolution

One question of interest concerning the lower 26-level vertical resolution is which vertical numerical approximations are more accurate, the finite difference associated with the Eulerian spectral transform or the Lagrangian with vertical remapping associated with the finite volume. Normally that would be interpreted as the simulation which matches the converged simulations more closely and one would conclude here in favor of the Lagrangian. However that conclusion cannot be drawn with these experiments because the parameterized forcing is very different between the 26-level and the higher resolution simulations. Thus the climate being simulated at higher resolution is in fact very different and unrelated to the climate simulated with 26-levels.

Table 1 shows that with the spectral transform model and increased vertical resolution there is a 10% increase over the 26-level simulation in the amount of water vapor transported into the equatorial region ($\varphi \leq |7.5|$). This is reflected in the difference of the integral of precipitation minus evaporation (P–E) there which represents the water vapor transported into the region. There is minimal variation in the average with the finite volume integrations with increasing vertical resolution. With the spectral transform integrations, the precipitation remains relatively unchanged while the evaporation decreases in the equatorial region. Following the arguments of Williamson and Olson (2003), the larger moisture transport into the equatorial region in the higher resolution spectral transform integrations leads to deep convection occurring sooner in a Lagrangian sense along the trajectory between the source outside the equatorial region and the equatorial region. The deep convection thus occurs at a more poleward latitude leading to the double structure in the precipitation in the higher resolution simulations. Once the precipitation sets up farther from the equator it becomes self reinforcing. The heating from the release of latent heat drives upward vertical motion and convergence into that region accompanied by divergence at the equator. The divergence draws water vapor away from the equator, preventing precipitation from forming on the equator. The higher resolution spectral transform model climate with the un-earth-like behavior in the subsidence region thus prefers the double structure.

6 Conclusions

Recently Williamson (2008a) showed that in Aqua Planet Experiment (APE) simulations with the 26-level Community Atmosphere Model version 3 (CAM3) the equatorial precipitation appeared to be converging with increasing horizontal resolution. However, the structure of the precipitation was different with the Eulerian spectral transform and with the finite volume dynamical cores, even though the parameterization suite was identical. The structure in the Eulerian spectral dynamical core simulation had a single precipitation maximum centered on the equator. That in the finite volume had double precipitation maxima spanning the equator with a minimum on the equator.

In this paper we examine the convergence with increasing vertical resolution from the 26 standard levels of CAM3 to 30 levels and 60 levels. Both versions of CAM3 do appear to be converging to the same state with increasing vertical resolution, the double precipitation maxima spanning the equator. With such a result one would normally assume that this double structure would be more correct for the lower resolution and that the finite volume dynamical core is more accurate at lower resolution. However we argue that that is not necessarily the case here because the parameterized forcing of the dynamical cores is very different at the higher vertical resolutions than at the low resolution. This yields a very different climate state at the different resolutions, particularly in the subsidence regions adjacent to the upward branch of the Hadley cell. This affects the moisture transport into the upward branch of the Hadley cell. At high resolution a very strong cloud layer develops around 900 mb which is not present at the low resolution. The cloud layer produces strong longwave radiative cooling of 14 K/day at the top of the cloud layer. Nevertheless, the parameterized specific humidity tendencies look very similar in the different resolution simulations.

We examine how the different state arises in the high resolution simulation by considering the evolution of a 60-level integration from an initial state taken from the 26-level simulation. In the 60-level evolution, the shallow convection initially turns off because at the increased vertical resolution the columns are stable by the discrete test upon which the parameterization is based. The PBL parameterization deposits water vapor between 850 and 900 mb. No other process removes that moisture. Thus the relative humidity increases and the relative humidity clouds start to form and increase in response to the moisture increase. The clouds lead to increased longwave radiation cooling which destabilizes the atmosphere enough so that the shallow convection then turns back on. The convection transports additional moisture upward

from the PBL deposition layer which leads to even more clouds and stronger radiative cooling in a vicious cycle. Ultimately the 60-level equilibrium is established in which the moisture tendencies from the PBL and shallow convection do not appear to be very different from the 26-level behavior. However, by then the atmospheric state no longer matches that of the low resolution model and the parameterized thermodynamic tendencies are different. The 60-level state is unrealistic compared to the earth's atmosphere. Similar unrealistic states have been seen in earth-like simulations with CAM3 at higher vertical resolutions. The 60-level aqua-planet state continues to have a large amount of low clouds which create excessive longwave cooling. The different state leads to different moisture transport into the equatorial region which drives the convection and favors the formation of the double structure.

With the higher vertical resolution, the shallow convection parameterization requires the unreasonable states in order to become active and thus appears to be inaccurate at higher vertical resolution. Normally, numerical approximations are expected to be more accurate at higher resolution. That is the case for many of the other parameterizations and for the dynamical core. Thus the shallow convection parameterization should be improved or replaced to allow increased vertical resolution in the model. It is being replaced in the next version of the CAM.

7 Acknowledgments

I would like to thank Richard Neale for comments on the original manuscript, Jim Hack for discussion on the parameterizations in the CAM and the anonymous reviewers for suggestions in improving the original manuscript. I would also like to thank Jerry Olson for developing the required code and running the experiments. This research was partially supported by the Office of Science (BER), U.S. Department of Energy, Cooperative Agreement No. DE-FC02-97ER62402.

References

- Boville, B. A., P. J. Rasch, J. J. Hack, and J. R. McCaa, 2006: Representation of clouds and precipitation processes in the Community Atmosphere Model version 3 (CAM3). *J. Climate*, **19**, 2184–2198.
- Collins, W. D., et al., 2004: Description of the NCAR Community Atmosphere Model (CAM3.0). NCAR Technical Note NCAR/TN-464+STR, National Center for Atmospheric Research, Boulder, Colorado. 214 pp., available from <http://www.ucar.edu/library/collections/technotes/technotes.jsp>.
- Collins, W. D., et al., 2006: The formulation and atmospheric simulation of the Community Atmosphere Model Version 3 (CAM3). *J. Climate*, **19**, 2144–2161.
- Hack, J. J., 1994: Parameterization of moist convection in the National Center for Atmospheric Research Community Climate Model (CCM2). *J. Geophys. Res.*, **99**, 5551–5568.
- Hannay, C., D. L. Williamson, J. J. Hack, J. T. Kiehl, J. G. Olson, S. A. Klein, C. S. Bretherton, and M. Köhler, 2009: Evaluation of forecasted southeast pacific stratocumulus in the NCAR, GFDL and ECMWF models. *J. Climate*, **22**, 2871–2889.
- Held, I. M. and M. J. Suarez, 1994: A proposal for the intercomparison of the dynamical cores of atmospheric general circulation models. *Bull. Amer. Meteor. Soc.*, **75**, 1825–1830.
- Holtslag, A. A. M. and B. A. Boville, 1993: Local versus nonlocal boundary-layer diffusion in a global climate model. *J. Climate*, **6**, 1825–1842.
- Kiehl, J. T., J. J. Hack, G. B. Bonan, B. A. Boville, B. P. Briegleb, D. L. Williamson, and P. J. Rasch, 1996: Description of the NCAR Community Climate Model (CCM3). NCAR Technical Note NCAR/TN-420+STR, National Center for Atmospheric Research, Boulder, Colorado. 152 pp.
- Klein, S. A. and D. L. Hartmann, 1993: The seasonal cycle of low stratiform clouds. *J. Climate*, **6**, 1587–1606.
- Lin, S.-J., 2004: A vertically Lagrangian finite-volume dynamical core for global models. *Mon. Wea. Rev.*, **132**, 2293–2307.

- Lin, S.-J. and R. B. Rood, 1996: Multidimensional flux-form semi-Lagrangian transport schemes. *Mon. Wea. Rev.*, **124**, 2046–2070.
- Lin, S.-J. and R. B. Rood, 1997: An explicit flux-form semi-Lagrangian shallow water model on the sphere. *Quart. J. Roy. Met. Soc.*, **123**, 2531–2533.
- Machenhauer, B., 1979: The spectral method. *Numerical Methods Used in Atmospheric Models, Vol. 2*, A. Kasahara, Ed., WMO and ICSU, Geneva, 121–275, GARP Publications Series No 17.
- Medeiros, B. and B. Stevens, 2010: Do aquaplanets describe the tropical atmosphere? *Clim. Dyn.*, **34**, submitted.
- Neale, R. B. and B. J. Hoskins, 2000: A standard test for AGCMs including their physical parameterizations. I: The proposal. *Atmos. Sci. Lett.*, **1**, 101–107.
- Rasch, P. J. and J. E. Kristjánsson, 1998: A comparison of the CCM3 model climate using diagnosed and predicted condensate parameterizations. *J. Climate*, **11**, 1587–1614.
- Simmons, A. J. and R. Strüfing, 1981: An energy and angular-momentum conserving finite-difference scheme, hybrid coordinates and medium-range weather prediction. ECMWF Technical Report 28, European Centre for Medium Range Weather Forecasts, Shinfield Park, Reading, Berkshire, UK.
- Williamson, D. L., 2008a: Convergence of aqua-planet simulations with increasing resolution in the Community Atmospheric Model, Version 3. *Tellus*, **60A**, 848–862.
- Williamson, D. L., 2008b: Equivalent finite volume and spectral transform horizontal resolutions established from aqua-planet simulations. *Tellus*, **60A**, 839–847.
- Williamson, D. L. and J. G. Olson, 2003: Dependence of aqua-planet simulations on time step. *Quart. J. Roy. Met. Soc.*, **129**, 2049–2064.
- Williamson, D. L., J. G. Olson, and B. A. Boville, 1998: A comparison of semi-Lagrangian and Eulerian tropical climate simulations. *Mon. Wea. Rev.*, **126**, 1001–1012.
- Zhang, G. J. and N. A. McFarlane, 1995: Sensitivity of climate simulations to the parameterization of cumulus convection in the Canadian Climate Centre general circulation model. *Atmos. Ocean*, **33**, 407–446.

Zhang, M., W. Lin, C. B. Bretherton, J. J. Hack, and P. J. Rasch, 2003: A modified formulation of fractional stratiform condensation rate in the NCAR Community Atmosphere Model (CAM2). *J. Geophys. Res.*, **108**, 4035, doi:10.1029/2002JD002523.

Figure Captions

Figure 1. Climatological zonal average precipitation for (a) spectral transform version and (b) finite volume version of CAM3 as a function of horizontal resolution with 26 levels. Grid points are indicated by dots.

Figure 2. Nominal pressures of 26-, 30- and 60-level grids below 500 mb.

Figure 3. Climatological zonal average precipitation as a function of vertical resolution for (a) T85 spectral transform and (b) 1° finite volume versions of CAM3. Grid points are indicated by dots.

Figure 4. Climatological zonal average (a) relative humidity, (b) cloud fraction, (c) longwave radiative heating, (d) PBL parameterization specific humidity tendency and (e) moist processes parameterization specific humidity tendency for T85 spectral transform CAM3 as a function of vertical resolution. Grid points are indicated by dots. The fields are averaged over the subsidence regions of the two hemispheres, $7.5^\circ \leq |\varphi| \leq 17.5^\circ$.

Figure 5. Two day evolution of 60-level model from a 26-level state for (a) temperature minus initial value, (b) specific humidity minus initial value, (c) relative humidity, (d) convective clouds (C_{CONV}), (e) relative humidity clouds (C_{RH}), (f) stratus clouds (C_{ST}), (g) cloud fraction, (h) cloud liquid water and (i) radiative heating. Except for (a-c) values are 1-hour averages ending at the hour indicated and the black dashed lines labeled “0 hr” are initial values from 26-level model. The fields are averaged over the subsidence regions of the two hemispheres, $7.5^\circ \leq |\varphi| \leq 17.5^\circ$.

Figure 6. Two day evolution of 60-level model from a 26-level state for parameterized specific humidity tendencies: (a) PBL, (b) shallow convection and (c) prognostic cloud water. Black dashed line labeled “0 hr” is initial value from 26-level model. Two day evolution from a 26-level state for fraction of points that are unstable in the shallow convection parameterization: (d) 26-level model and (e) 60-level model. Values plotted are 1-hour averages ending at the hour indicated. The fields are averaged over the subsidence regions of the two hemispheres, $7.5^\circ \leq |\varphi| \leq 17.5^\circ$.

Figure 7. Moist static energy (solid line) and saturated moist static energy (dashed line) at a single point (longitude 243.3° and latitude 7.7°) for 26-level model at (a) hour 0, and 60-level model at (b-f) hours 0, 1, 2, 3, and 6 respectively. Vertical lines elevate the moist static energy to the next higher grid level. Grid points are indicated by dots.

Table 1: Equatorial averages over latitudes $|\varphi| \leq 7.5$ of precipitation (PRECIP), evaporation (EVAP) and precipitation minus evaporation (P-E) (mm/day).

RESOLUTION	SPECTRAL TRANSFORM			FINITE VOLUME		
	PRECIP	EVAP	P-E	PRECIP	EVAP	P-E
26 LEVELS	11.6	4.4	7.2	11.5	3.9	7.6
30 LEVELS	11.5	3.6	7.9	11.1	3.8	7.4
60 LEVELS	11.7	3.8	7.9	11.6	4.1	7.5

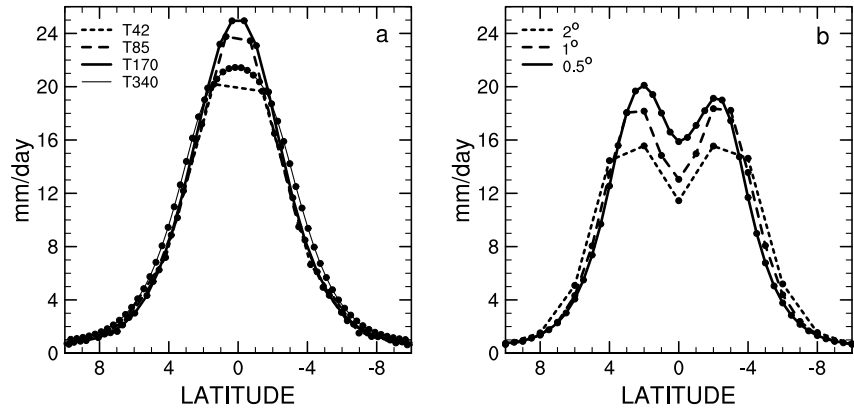


Figure 1: Climatological zonal average precipitation for (a) spectral transform version and (b) finite volume version of CAM3 as a function of horizontal resolution with 26 levels. Grid points are indicated by dots.

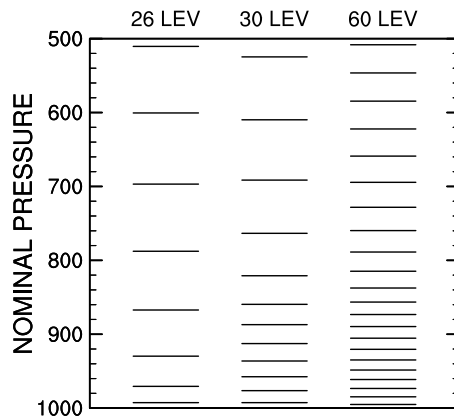


Figure 2: Nominal pressures of 26-, 30- and 60-level grids below 500 mb.

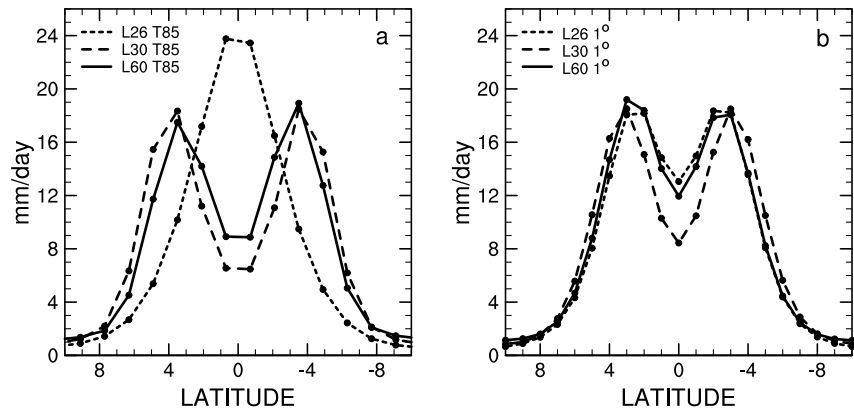


Figure 3: Climatological zonal average precipitation as a function of vertical resolution for (a) T85 spectral transform and (b) 1° finite volume versions of CAM3. Grid points are indicated by dots.

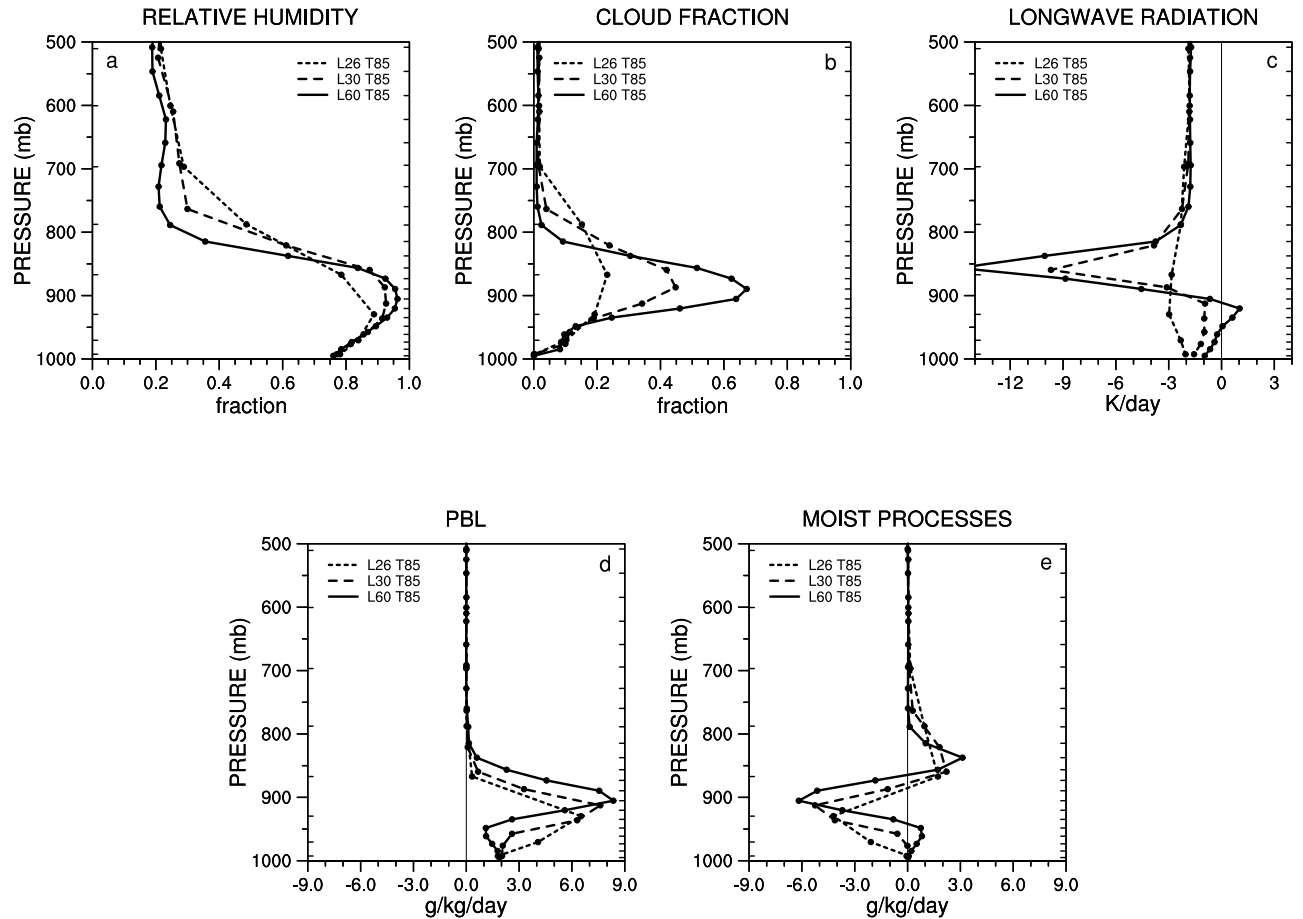


Figure 4: Climatological zonal average (a) relative humidity, (b) cloud fraction, (c) longwave radiative heating, (d) PBL parameterization specific humidity tendency and (e) moist processes parameterization specific humidity tendency for T85 spectral transform CAM3 as a function of vertical resolution. Grid points are indicated by dots. The fields are averaged over the subsidence regions of the two hemispheres, $7.5^\circ \leq |\varphi| \leq 17.5^\circ$.

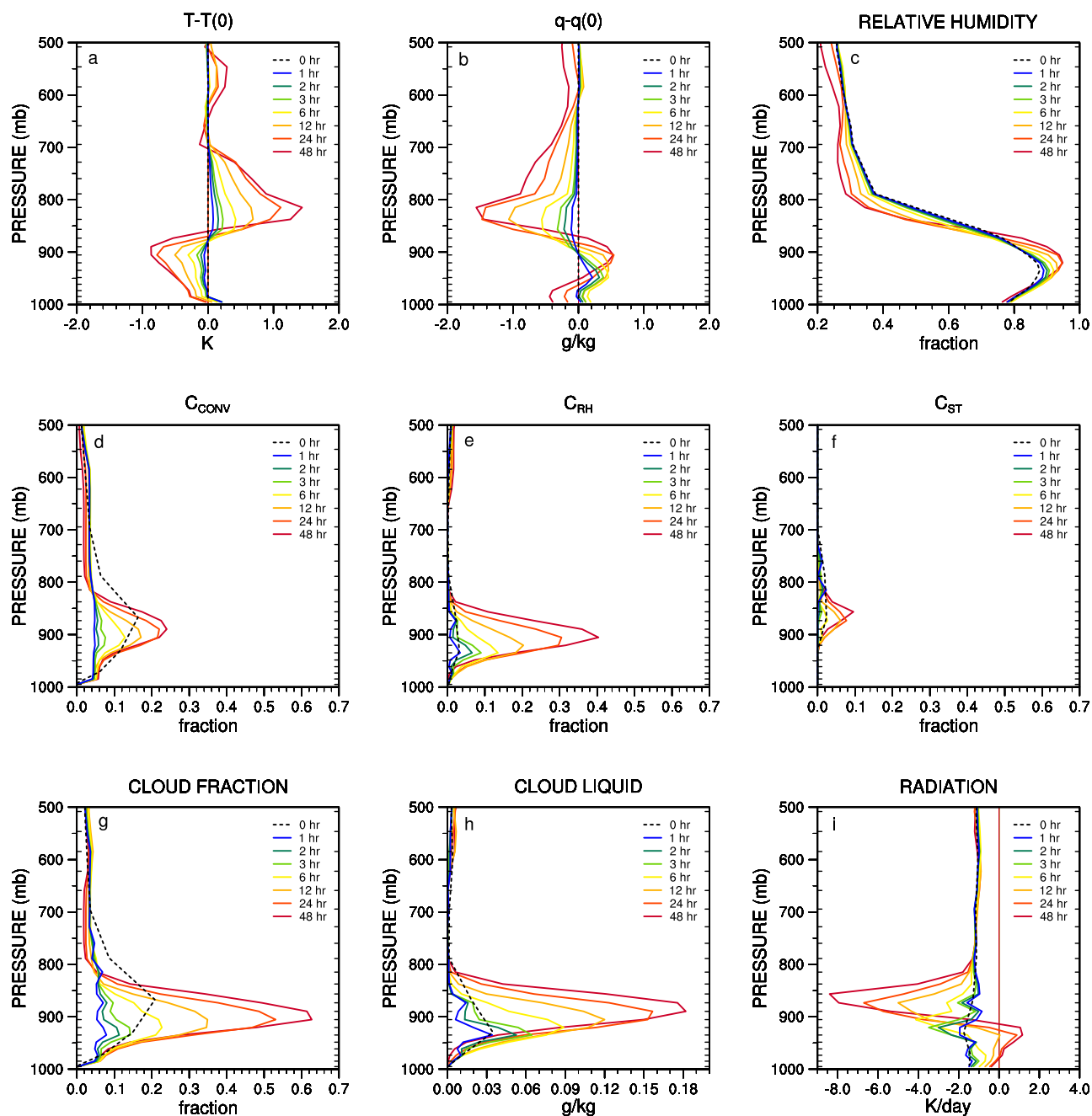


Figure 5: Two day evolution of 60-level model from a 26-level state for (a) temperature minus initial value, (b) specific humidity minus initial value, (c) relative humidity, (d) convective clouds (C_{CONV}), (e) relative humidity clouds (C_{RH}), (f) stratus clouds (C_{ST}), (g) cloud fraction, (h) cloud liquid water and (i) radiative heating. Except for (a-c) values are 1-hour averages ending at the hour indicated and the black dashed lines labeled “0 hr” are initial values from 26-level model. The fields are averaged over the subsidence regions of the two hemispheres, $7.5^\circ \leq |\varphi| \leq 17.5^\circ$.

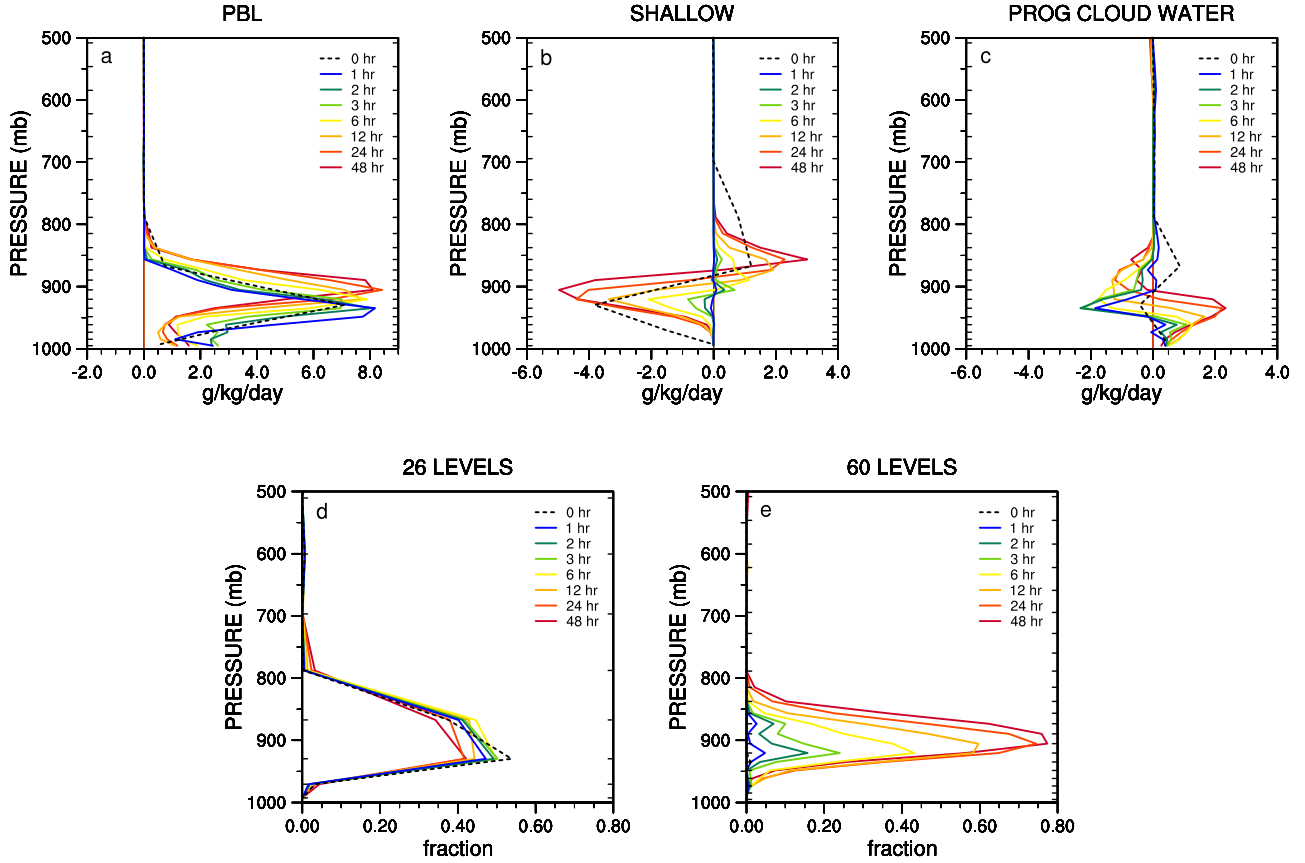


Figure 6: Two day evolution of 60-level model from a 26-level state for parameterized specific humidity tendencies: (a) PBL, (b) shallow convection and (c) prognostic cloud water. Black dashed line labeled “0 hr” is initial value from 26-level model. Two day evolution from a 26-level state for fraction of points that are unstable in the shallow convection parameterization: (d) 26-level model and (e) 60-level model. Values plotted are 1-hour averages ending at the hour indicated. The fields are averaged over the subsidence regions of the two hemispheres, $7.5^\circ \leq |\varphi| \leq 17.5^\circ$.

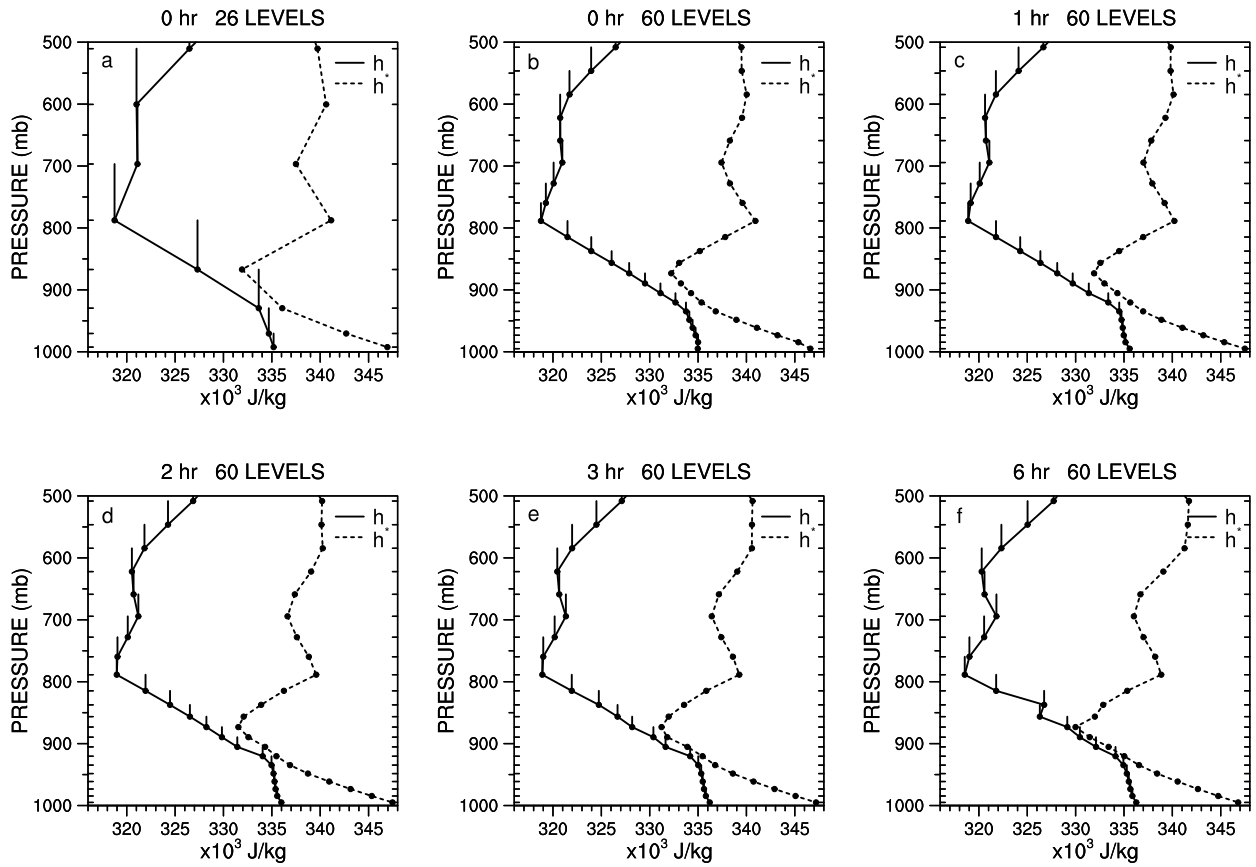


Figure 7: Moist static energy (solid line) and saturated moist static energy (dashed line) at a single point (longitude 243.3° and latitude 7.7°) for 26-level model at (a) hour 0, and 60-level model at (b-f) hours 0, 1, 2, 3, and 6 respectively. Vertical lines elevate the moist static energy to the next higher grid level. Grid points are indicated by dots.